ChemPubSoc Europe
DOI: 10.1002/cctc.201700753
CHEMCATCHEM Full Papers

Origin and Abatement of Heterogeneity at the Support Granule Scale of Silver on Silica Catalysts

Eva Plessers,[a] Jeroen E. van den Reijen,[b] Petra E. de Jongh,[b] Krijn P. de Jong,[b] and Maarten B. J. Roeffaers*[a]

Incipient wetness impregnation is used commonly to form supported metal nanoparticle catalysts. Recently, it has been revealed that this approach may induce severe heterogeneity between catalyst granules of the same batch. At least a 10-fold variation in metal loading was observed, which affect the catalytic performance of individual catalyst granules severely. However, the origin of this heterogeneity is still unclear. Here we show that every elementary step in the preparation procedure of a Ag on silica catalyst has an effect on the resulting interparticle heterogeneity, but the influence of the drying step is the most important. This is because drying by capillary force results in a heterogeneous sample. Specifically, the position of a granule in the stagnant drying bed influences the resulting color and, thus, Ag loading significantly. This is further demonstrated by varying the drying conditions: freeze-drying and fluidized-bed drying led to a more homogeneous Ag loading. An investigation of the fluidized-bed-dried sample by using optical microscopy revealed a large fraction of transparent granules (94%), which indicates that almost all the Ag nanoparticles in this sample are confined within the 6 nm pores. The optimized supported Ag on silica catalyst shows a good catalytic performance. This adaptation of the drying step can be implemented easily on a laboratory scale, is scalable, and does not require the use of expensive solvents or metal precursors.

Introduction

Supported metal nanoparticles are widespread in heterogeneous catalysis as they combine both a high activity and stability. These metal nanoparticle catalysts are also used commonly in catalyst discovery research on a laboratory scale and are often prepared by incipient wetness impregnation (IWI). Generally, the preparation method influences the final catalytic performance significantly as the metal nanoparticle size and distribution inside the support depend on the preparation method.[1–6] This was the driving force for the development and application of various characterization techniques. The characterization methods used most frequently, such as XRD, chemisorption, extended X-ray absorption fine structure analysis, and UV/Vis diffuse reflectance spectroscopy,[7–13] yield average nanoparticle sizes. This value reveals little to no information about nanoparticle distribution and/or dispersion within a single and between different micrometer- or millimeter-sized support granules. Conversely, if we zoom in on the nanoparticles by using TEM we can obtain a precise determination of individual supported nanoparticle dimensions and distributions if a representative sample of the powder is investigated.[1,14,15] Besides electron microscopy, a wide variety of X-ray-based imaging techniques have been developed to study the heterogeneity of solid catalysts.[16–20]

For industrial-scale millimeter-sized support bodies, it is known that non-uniform metal loadings such as "egg–shell", "egg–yolk", or "egg–white" are generally obtained more than a "uniform" homogeneous distribution.[3,6,21–23] From previous reports and model calculations, Morbidelli et al.[21] conclude that several experimental factors, for example, precursor solution concentration, pH, ionic strength, temperature, and drying conditions, cause this heterogeneity during the preparation of supported metal catalysts. Additionally, for micrometer-sized granules that are used typically for catalyst discovery on a laboratory scale, intraparticle variations in nanoparticle size, dispersion, and distribution have been shown. The use of electron tomography, for example, revealed that typical impregnation and drying results in a non-uniform metal distribution and nanoparticle size, whereas optimization of drying and calcination resulted in a more homogeneous loading.[14,24–26] However, to the best of our knowledge, studies on interparticle heterogeneities at the support granule level have only been reported twice: (1) advanced electron tomography on Pt-loaded submicron USY zeolites[1] and (2) a correlative approach by using optical microscopy on Ag-loaded mesoporous silica granules.[2] In both cases, at least a 10-fold variation in metal loading between different support particles was found. Furthermore, these differences in the metal loading were shown to affect the catalytic performance severely if the same granule scale

[a] Dr. E. Plessers, Prof. Dr. M. B. J. Roeffaers
Centre for Surface Chemistry and Catalysis
KU Leuven
Celestijnenlaan 200f, 3001 Heverlee (Belgium)
E-mail: marten.roeffaers@kuleuven.be

[b] J. E. van den Reijen, Prof. Dr. P. E. de Jongh, Prof. Dr. K. P. de Jong
Inorganic Chemistry and Catalysis,
Debye Institute for Nanomaterials Science
Utrecht University
Universiteitsweg 99, 3584 CG Utrecht (The Netherlands)

Supporting information and the ORCID identification number(s) for the author(s) of this article can be found under: https://doi.org/10.1002/cctc.201700753.

was measured.[2] In contrast to millimeter-sized support bodies, in which the transport of the metal precursor by the impregnation solution during drying is responsible for the heterogeneous metal loading, the origin of the heterogeneity during the preparation of supported nanoparticles at micrometer-sized granules has not yet been investigated.

In this work, optical microscopy was used to study the influence of the different elementary steps on the loading heterogeneity during the preparation of supported Ag on micrometer-sized silica granules. Typical impregnation procedures and a silver nitrate precursor solution that displays limited chemical or electrostatic interactions with the support are used. Variations in Ag loading at the granule level were assessed from the coloration of individual support granules within the resulting powder. From our results, we conclude that each of the elementary steps, namely, impregnation, drying, calcination, and activation, induces interparticle heterogeneity at the granule level. For this particular support and metal (precursor) system, the drying step causes most of the heterogeneity. Specifically, we also show how fluidized-bed drying abates most of the heterogeneity in loading effectively; this optimized drying method can be implemented easily into the preparation of supported metal catalysts. The optimized supported Ag on silica catalyst shows a good catalytic performance.

Results

First, 5 wt% Ag supported on a silica gel (Sigma–Aldrich, Fluka 60752) with a 409 $m^2 g^{-1}$ BET specific surface area and 6 nm pore diameter was prepared by standard IWI from a 3.6 mM silver nitrate solution.[3,5,6] After calcination, the resulting silica-supported Ag nanoparticle powder has a typical yellowish color and homogeneous appearance. However, as reported before,[2] optical microscopy revealed an unexpected color variability with support granules, which ranged from transparent to yellow to red. The color at the support granule level is associated with the Ag nanoparticles, specifically to the surface plasmon resonance. This plasmon absorbance is determined largely by the nanoparticle size, nanoparticle shape, and refractive index of the environment.[27] An increase of the Ag nanoparticle diameter inside a silica matrix from below 10 nm to approximately 100 nm results in a redshift of the surface plasmon resonance absorbance peak from 420 nm to approximately 520 nm and a change in color from weak yellow to intense red.[8] However, not only the size but also the Ag nanoparticle concentration will influence the overall optical appearance of the support granule. As evidenced before by the correlation of the results obtained by using optical microscopy with high-resolution SEM and energy-dispersive X-ray spectroscopy (EDX), the coloration of our Ag on silica sample is related to both the nanoparticle loading and size.[2] Transparent granules contain a low concentration of pore-confined 6 nm Ag nanoparticles, whereas an increased coloration was associated with an elevated Ag concentration and the formation of large Ag nanoparticles on the outer surface of the granules.

Although the interparticle heterogeneity in Ag loading at the silica support granule level has been reported before,[2] the origin of this heterogeneity is still unclear. To identify the cause, four possible origins of heterogeneity were evaluated in detail: (1) variability between support granules in surface charge or metal impurities; and heterogeneity induced during (2) impregnation, (3) drying, and (4) calcination (Figure 1). The influence of each of these parameters on the resulting interparticle heterogeneity was assessed from the color heterogeneity of the powder obtained after the last calcination and activation step.

Heterogeneity at the support granule level

Variability in surface charge density

Generally, the adsorption strength of the metal precursor onto the support plays an important role during impregnation,[6,21,28] and the variability in surface charge between support granules might be the first possible origin of the observed heterogeneity. For the studied system, Ag cations show a weak adsorption onto the silica support surface because of the limited surface charge density at the prevailing pH.[21,29] Silica immersed in neutral water acquires some negative surface charges of approximately $-0.02\ C\,m^{-2}$,[30] predominantly through the deprotonation of terminal silanol groups.[31] For 1 g of silica gel with a BET specific surface area of 409 $m^2 g^{-1}$, this corresponds to 85 μmol of negatively charged O atoms on the surface. To prepare a 5 wt% Ag on silica material, a solution with 460 μmol ionic Ag is used, so that for this specific system less than 20% of the total amount of Ag ions can be adsorbed electrostatically on the silica surface. To test the hypothesis, the surface charge density of the support granules was probed by investigating the ion exchange of a cationic dye Rhodamine 6G. From the reported silica surface charge density,[30] the silica gel powder was contacted with an aqueous Rhodamine 6G solu-

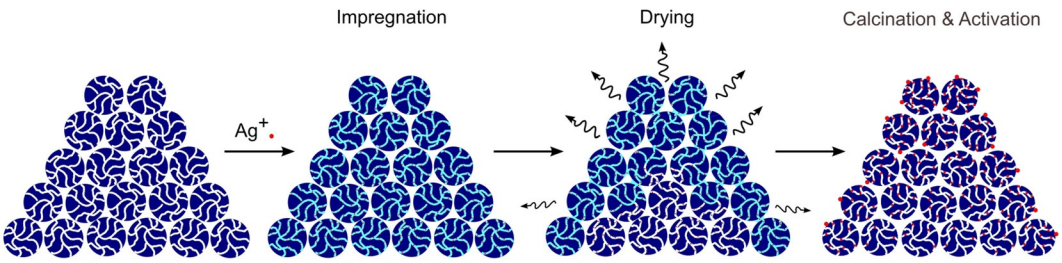

Figure 1. Schematic representation of IWI followed by drying and calcination.

tion that contained sufficient cationic dye to compensate all theoretical surface charges (Figure S2).

We used confocal microscopy with a 405 nm laser to conclude that there is a fivefold variability in the Rhodamine concentration between different support granules. As this interparticle heterogeneity in Rhodamine loading is a direct measure for the surface charge heterogeneity, this can only explain the observed 10-fold heterogeneity in Ag loading between different silica support granules partially.[2] Although, as mentioned above, only less than 20% of the Ag ions at this loading of 5 wt% can be adsorbed electrostatically on the silica surface and this factor will become important if catalysts are prepared with low loadings of (noble) metals.

The heterogeneity in surface charge could have various origins, of which differences in silanol density amongst the different silica gel particles is the most plausible. In an attempt to homogenize the surface charge, the silica gel was pretreated with an aqueous 0.1 M NaOH solution followed by extensive washing with distilled water before impregnation (see Supporting Information). This treatment should deprotonate all surface hydroxyl groups to the same extent. If we used the preactivated silica support in the regular IWI procedure, the bulk powder showed a reduced yellow coloration (Figure 2b), which was confirmed by using optical microscopy. Clearly, silanol activation decreases surface charge heterogeneity. Unfortunately, the base pretreatment results in partial silica dissolution and fragmentation that makes a detailed comparison at the single support particle level, for example, by Rhodamine 6G staining, difficult. However, the experiment does support the idea of particle-to-particle variations in silanol density.

Metal impurities

Besides intrinsic heterogeneities in surface charge density, metal impurities (e.g., Na, Al, Ti) present in the silica gel before impregnation also influence the overall surface charge severely. As silica gel is made typically from impure water glass solutions,[4] the IWI procedure was repeated using a self-synthesized silica gel made from tetraethyl orthosilicate (TEOS) and an ultra-pure silica (CARiACT) obtained commercially (see Supporting Information). The thus obtained powders showed a dark coloration (Figure 2c and d). If we zoom in at the support granule level, an even larger heterogeneity than that of the standard silica gel support was observed, which shows that the presence of impurities is not the origin of the observed heterogeneity. As these different silica materials have a different surface area, grain size, and pore size, a detailed one-to-one comparison is not possible. Further impregnation studies described in this work were, therefore, always executed with the commercial silica gel (obtained from Sigma–Aldrich) with a pore diameter of 6 nm and a granule size of 40–75 μm.

Heterogeneity induced during impregnation

Coimpregnation

As variation in the surface charge at the granule level can partially explain the observed heterogeneity in Ag loading, a coimpregnant can be introduced in the impregnation solution to compete with the cationic Ag for the negatively charged adsorption sites. For example, this strategy is often used for Pt impregnation into Al_2O_3 pellets.[4,21] The effect of coimpregnation with an excess of ammonium nitrate was investigated. However, this procedure did not lead to complete homogeneity (Figure S3).

Pore filling

An important question in the conventional IWI procedure is if all pores are filled effectively with the precursor solution. Uneven pore filling could also cause a difference in metal loading at the support granule level. A positive indication of complete pore filling, often used in the laboratory, is the sudden transition of a seemingly "dry" powder to a moist state upon addition of the last drop of the precursor solution.[5] As the correct determination of the support mesopore volume is an important parameter to reach this situation, N_2 physisorption was performed on the silica gel supports under study (see Supporting Information). The use of an impregnation solution with a volume that equals the pore volume determined by using N_2 physisorption precludes that up until the addition of the last drop of the precursor solution, capillary forces drive the uptake of the solution into the support. However, careful execution and macroscopic observation of the impregnation step indicated that vigorous stirring as the precursor solution is added is very important to maintain the dry powder state until the last drop. We used macroscopic examination to indicate that complete pore filling was reached, as only at the very last

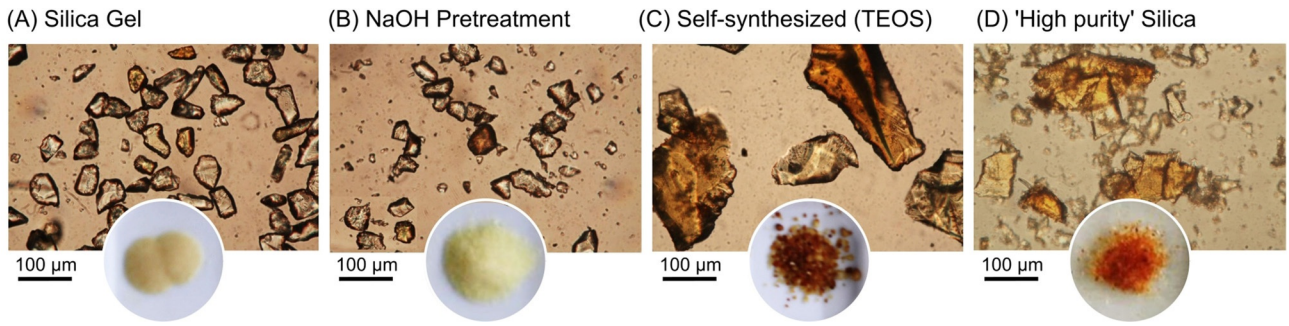

Figure 2. Ag IWI on various silica supports: A) standard silica gel (Aldrich), B) NaOH-preactivated silica gel, C) TEOS-based self-synthesized silica gel, and D) high-purity silica (CARiACT; 5–6 wt% Ag, vacuum drying at room temperature for 16 h, calcination 16 h at 500 °C).

drop all pores are filled and the system changes to a moist state, and pore filling during impregnation is thus not the origin of heterogeneity. Furthermore, different techniques have been reported previously that also confirm that pore filling was homogeneous after impregnation.[25,32]

Although impregnation under vacuum conditions is known to be beneficial for the resulting homogeneity, this is difficult practically if micrometer-sized granules are used.

Wet impregnation

Besides IWI, another impregnation method used frequently is "wet impregnation" or "diffusional impregnation" in which the support is wetted with pure solvent before impregnation with the precursor solution.[4,6] Wet impregnation was executed to test if the interparticle heterogeneity could be decreased. A visual inspection of the powder obtained by wet impregnation after the calcination step, however, suggests an even larger heterogeneity because of the dark yellow color of the obtained bulk powder. As mentioned above, the intensity of the plasmon absorbance of Ag nanoparticles decreases upon decreasing their size, whereas an increasing size results in a more intense and redshifted absorbance. In addition, Ag loading determines the color of the resulting powder. Close inspection by using optical microscopy revealed the fraction of dark colored orange to red granules that contained excessive amounts of Ag and that the amount of larger Ag nanoparticles is increased strongly (from 0.5 to 2.6%). The complete color distribution among the individual supported Ag granules as observed by using optical microscopy is shown in Figure 3b.

Heterogeneity induced during drying

Alternative drying methods

Typically, drying after impregnation is performed in a static oven, however, metal precursor redistribution within and between support granules might occur. To minimize the redistribution of metal precursor within individual support granules and to optimize metal dispersion, alternative drying methods, such as freeze-drying or vacuum drying, have been explored.[14,33] Based on these earlier findings, the influence of vacuum drying and freeze-drying on the resulting color heterogeneity at the granule scale for our Ag on silica powder was evaluated. From the color distribution shown in Figure 3c it is clear that vacuum drying has a positive effect. Not only does it increase the fraction of light yellow colored granules (from 24 to 29%) but also the fraction of dark orange to red granules decreases similarly (from 0.5 to 0.4%). An even more homogeneous color distribution at the granule scale was obtained after freeze-drying (Figure 3d).

Drying bed

Clearly, the drying conditions of the freshly impregnated powder play an important role. Within the static drying bed temperature and concentration gradients might develop. To examine the influence of the position of a support granule in the drying bed on the resulting color and thus Ag loading, the powdered bed was sliced in half after drying and calcined as the powder configuration was maintained carefully (Figure 4a–d). The overview picture taken of the powdered bed after calcination (Figure 4e–h) shows clearly that granules that were present in the interior of the bed during drying are markedly less colored than granules that resided closer to the exterior of the bed. This observation conflicts with the general assumption that during drying, metal precursor precipitation takes place within or at the outside of the original granule and no migration between granules exists; notably, within one support granule precursor migration has been observed before.[14,24–26]

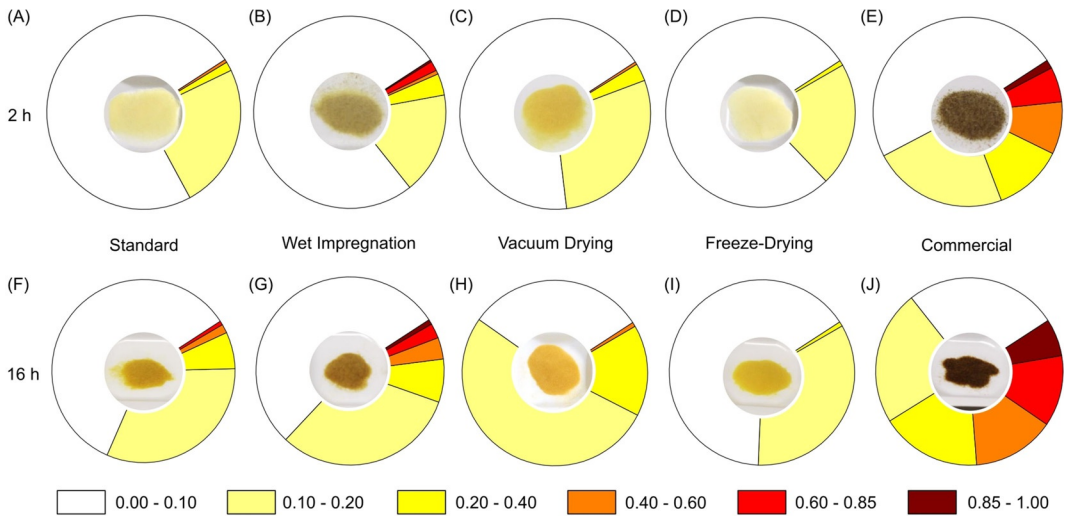

Figure 3. Schematic representation of the color distribution at the catalyst granule level as a result of varying the preparation conditions (5–6 wt% Ag, calcination 2 h (top) and 16 h (bottom) 500 °C). Color heterogeneity ($n = 250$) illustrated with a pie diagram, colors represent the color index of individual Ag/SiO_2 granules (for determination see Supporting Information and Ref. [2]).

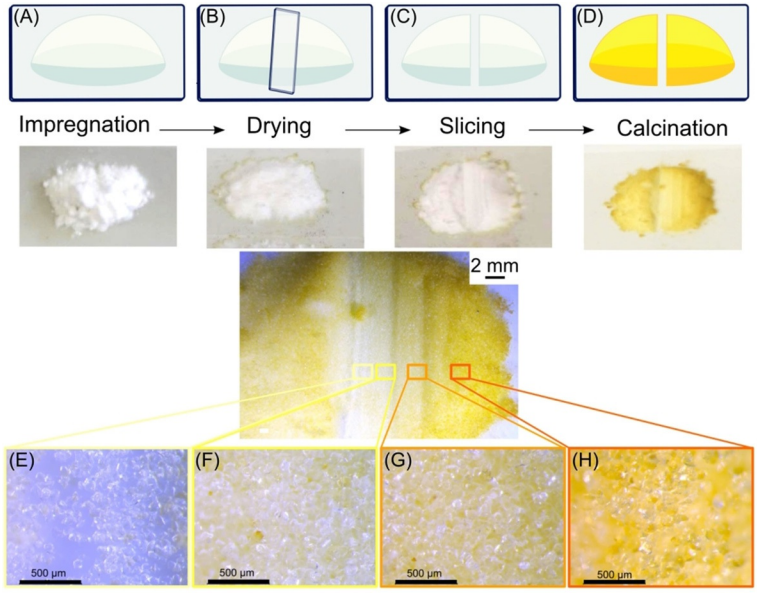

Figure 4. Influence of position in the drying bed. After A) impregnation and B) drying, C) the powder is sliced, D) during calcination the sliced configuration is maintained, G,H) optical examination of the calcined powder reveals granules present in the exterior of the drying bed are predominantly yellow to orange colored, whereas E,F) the granules present in the interior of the bed are mostly transparent.

Fluidized-bed drying

To prevent the directional transport of the metal precursor between support granules as observed during static drying, an alternative to static drying was investigated. de Jong and coworkers have explored fluidized-bed drying approaches to improve the Co distribution within mesoporous silica upon impregnation with $Co(NO_3)_2$.[26] The impregnated powder is loaded into a tubular reactor through which a gas is flowed from bottom to top to create a fluidized bed. The effect of this drying method on the resulting color heterogeneity was tested by drying freshly prepared Ag-impregnated silica under an air flow (30 mL min^{-1}, 80% N_2, 20% O_2) at 100 °C for 8 h. Macroscopically, the obtained powder appears lightly colored, which indicates a more homogeneous Ag distribution. This was also confirmed by using optical transmission microscopy. The color distribution in the sample is shown in Figure 5a. The fraction of transparent granules increased significantly from 74 to 94%, and the average Ag loading is maintained.

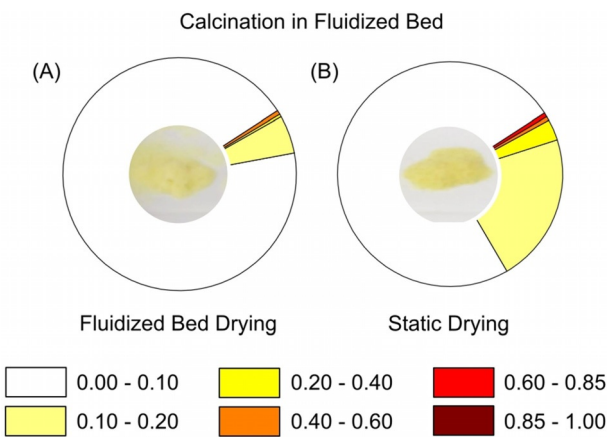

Figure 5. Color distribution in Ag/SiO_2 after A) fluidized-bed drying and B) static drying followed by calcination in a fluidized bed (drying 100 °C 8–16 h; calcination 1 °C min^{-1} at 500 °C^{-2} h).

Both fluidized-bed drying and fluidized-bed calcination can be at the origin of the improved homogeneity of the powder. Subsequently, a traditionally dried Ag on silica powder (100 °C static, 16 h) was calcined under similar fluidized-bed conditions (air flow 30 mL min^{-1}, 80% N_2, 20% O_2, 1 °C min^{-1} to 500 °C, 2 h). The obtained powder resembles strongly that obtained by following the standard impregnation procedure (Figures 5b and 2a). The remarkable increase in homogeneity can hence be attributed to the fluidized-bed drying. Notably, also under these conditions, the drying temperature plays a crucial role.[26,33] For this particular system, a drying temperature of 100 °C gave the best results.

Heterogeneity induced during calcination

Calcination time

From the experiments discussed above, calcination seems not to play a decisive role in the final coloration of the silica-supported Ag powder, that is, in comparison between the fluidized-bed and static calcination of the standard dried catalysts. However, a different calcination time might affect the heterogeneity of the samples as at this stage the final nanoparticles are formed. To test this hypothesis, the calcination time was increased from 2 to 16 h. The increase in coloration of the sample is significant (Figure 3a–e vs. f–j, top vs. bottom row). The prolonged calcination induces a transition from uncolored 6 nm pore-confined Ag nanoparticles to larger (colored) Ag nanoparticles formed on the outer surface of the granules. Even though the calcination temperature of 500 °C is well below the melting temperature of Ag (962 °C),[34] metal mobility is known to start already at half the melting point, the so-called Tamman temperature. However, nanoparticles do not generally migrate but rather diffuse around their initial position. In our sample relatively low loadings are used to result in relatively large inter-nanoparticle distances, so nanoparticle movement and coalescence is most likely not the reason for the particle growth. However, during calcination in air Ag is oxidized partially to Ag ions.[35] These Ag ions are highly mobile and can migrate between Ag nanoparticles, which leads to particle growth.

Calcination bed

The particle growth phenomenon, similar to the heterogeneities as a consequence of the drying step, might also be related to the relative position of the granule inside the powdered bed during the calcination (see Supporting Information). To test this hypothesis, well-dispersed individual granules were

calcined in an in situ heating stage with minimal temperature gradients. We used optical microscopy to observe that color heterogeneities are still present (Figure S4). The color heterogeneities that develop under such conditions are caused by the variability induced by the previous steps in the IWI procedure (vide supra).

Catalysis

To test the impact of the improved homogeneity after fluidized-bed drying on catalysis, the catalytic performance of this sample was compared to that prepared by the standard IWI procedure (Table 1). Single support particle catalytic experiments have already been used to reveal a large particle-to-particle variation in catalytic performance in the chemoselective hydrogenation of 4-nitrostyrene.[2] This reaction was chosen for the bulk catalytic experiments. The standard and fluidized-bed-prepared Ag/SiO_2 samples were crushed before reaction to eliminate mass transport effects, put in the high-pressure reactor together with the substrate (4-nitrostyrene, 2 mol% Ag), internal standard (tetradecane), solvent (EtOH), and pressurized to 20 bar with H_2 after flushing the reactor with N_2. After 30 min at 140 °C, the reaction was stopped, and the products were analyzed by using GC. The samples prepared by fluidized-bed drying outperform the standard IWI-prepared material.

Table 1. Results of the catalytic hydrogenation of 4-nitrostyrene (X = conversion, S = selectivity).

Reaction[a]	t [h]	X [%]	$S_{4\text{-Van}}$ [%][b]	$S_{4\text{-Ean}}$ [%][c]
Standard preparation	0.5	41	95	2
Fluidized bed	0.5	53	93	4

[a] Reaction conditions: 100 °C, 20 bar of H_2, 2 mol% Ag, 0.13 M 4-nitrostyrene in EtOH, 500 rpm. [b] 4-Van = 4-vinylaniline. [c] 4-EAn = 4-ethylaniline.

Discussion

The Rhodamine 6G experiments demonstrate clearly the presence of interparticle heterogeneity in surface charge between the individual silica support granules even before impregnation. This interparticle heterogeneity originates from the calcination step in the preparation of the dry silica gel. Temperature gradients from the outside towards the inside of the wet gel develop; in the outer regions more severe heating results in a more drastic dehydration and hence a loss of surface hydroxyl groups. After calcination, the solidified gel is crushed into micrometer-sized granules used to support the metal nanoparticles. As the whole individual micrometer-sized support granule originates from one position within the calcined gel, only limited intraparticle heterogeneities in surface hydroxyl groups can be expected within the granule. Moreover, interparticle heterogeneities are expected for the same reason as these support granules might originate from different regions of the original wet and calcined gel. This is supported by the Rhodamine 6G experiment that shows a fivefold variation in surface hydroxyl density between individual granules and no severe variations within the particles.

The experiments in which we focused on the drying step after impregnation reveal that drying has a significant influence on the resulting color heterogeneity. The influence of the drying step on the resulting metal dispersion and distribution inside and on the support has been studied extensively at the millimeter-size support body level.[21] The two factors that determine the final metal loading are (1) convective flow from the inside of the body towards the outer surface induced by evaporation and (2) diffusive transport induced by concentration gradients. Fast drying minimizes such effects and leads to the maximal preservation of the metal precursor distribution inside the support body.[21] However, studies have indicated that for weakly adsorbed metal precursors, accumulation of the precursor at the external surface of the support body is significant even with fast drying.[36] This results in the so-called egg–shell metal distribution.[3,6] The final metal distribution in the support bodies is, thus, determined by the relative strength of convection, diffusion, and adsorption and it can be influenced by a variety of parameters, such as the viscosity and pH of the solution, solubility of the precursor, adsorption strength, and size of the support.[3,6,36] To rule out the latter, laboratory-scale nanoparticle catalysts are often supported on micrometer-sized granules and it is believed that these phenomena are not important in contrast to that on millimeter-sized industrial pellets.[3] The coloration as a function of the position in the drying bed (Figure 4) refutes this general assumption clearly. Although the convective and diffusional transport of Ag between different granules seems unlikely, these experiments show that silver nitrate transport during drying towards the "evaporative zone" happens.

As the granule color is related to Ag loading and the size of the Ag particles on the outer surface of the granule, a homogeneous color distribution originates from both an equal Ag loading inside all the individual granules and the formation of only pore-confined 6 nm Ag nanoparticles. The more homogeneous color distribution as the result of freeze-drying can be attributed to the fixation of the solvent to the granules, which restricts the exchange of solution between two adjacent granules and is, thus, a good indication of equal loading. Additionally, during freeze-drying there is no liquid–gas interface and hence no capillary effects. Under normal drying conditions, a meniscus is formed, which ensures that upon drying larger pores are emptied first, whereas smaller pores remain filled with solution, and the meniscus retracts to the smaller pores to cause the redistribution of the active material. Therefore, freezing prevents the migration of the silver nitrate during drying, so more of the Ag nanoparticles are located inside the support granule and fewer large Ag particles are formed on the outer surface. The beneficial effect of restricting the exchange of solution between two adjacent granules is further evidenced by the large fraction of transparent granules (94%) after fluidized-bed drying. The transparent color does not indicate that all these granules have a very low Ag loading as the

same initial Ag salt concentration is used in all impregnated samples. The Ag nanoparticles inside the transparent granules in the fluidized-bed sample are thus all present as pore-confined 6 nm sized nanoparticles. Conversely, in the wet impregnated sample, it is more likely that larger Ag nanoparticles form on the outer surface to give rise to a higher fraction of orange and red colored granules (2.6%). Furthermore, fluidized-bed drying and freeze-drying randomizes the granules within the drying bed. This granule randomization also counters the effect of temperature gradients that develop during traditional drying. The fact that the position inside the drying bed plays such an important role during the IWI procedure has probably been overlooked because of the randomization of the granule positions between the different steps that is, the dried powder is transferred typically to a heat-resistant crucible for calcination, which removes the direct link between the final properties and the location. The optimized Ag distribution obtained by fluidized-bed drying also resulted in an improved catalytic performance because of the more efficient use of the impregnated Ag.

Conclusions

Optical microscopy was used as a characterization tool to improve the incipient wetness impregnation of Ag nanoparticles supported on silica gel. Variations in Ag loading were assessed from the color of individual support granules within the resulting powder. The use of other silica support materials, wet impregnation, and prolonged calcination in air induced an even larger interparticle color heterogeneity at the support granule scale. Conversely, by changing the drying conditions to fluidized-bed drying, a nearly homogeneous sample was obtained. A comparison of the resulting granule color and its position in the static drying and calcination bed revealed the significant impact of temperature gradients and Ag nitrate transport across the bed on the heterogeneity. In fluidized-bed drying, the position of the individual granules is randomized continuously to eliminate this impact. During freeze-drying, the exchange of solution between two adjacent granules is restricted to lead to a homogeneous loading. Additionally, freezing prevents the migration of silver nitrate to the surface during drying to result in more Ag nanoparticles located inside the support granule and fewer large Ag particles at the outer surface of the silica. This is even more pronounced in fluidized-bed drying: the large fraction of transparent granules (94%) indicates that almost all the Ag nanoparticles in this sample are pore-confined 6 nm nanoparticles. The optimized supported Ag on silica catalyst showed an excellent catalytic performance, which supports previous observations made at the single support particle level.[2] Interestingly, this adaptation to the drying step of the incipient wetness impregnation procedure can be implemented easily on the laboratory scale, is scalable, and does not require the use of expensive solvents or metal precursors.

Future work will involve the determination of single-particle Ag loading and size and distribution characterization both at the outer surface and inside the granules, which requires the use of additional characterization techniques, such as energy-dispersive X-ray spectroscopy, SEM, and TEM, combined with 3D representation or sectioning. This work demonstrates that such detailed characterizations are best repeated whenever changes to the incipient wetness impregnation procedure are implemented. For example, it can be expected that catalysts with low loadings will suffer from the intrinsic variation in surface charge at the granule level. The power of optical microscopy is that simple and fast observation can be combined easily with other more advanced characterization techniques.[2,37,38] Furthermore, optical screening could become a general technique to study catalyst preparation procedures as it can be used equally for a variety of other metals and metal oxides that also develop colors such as Au, Cu, Pt, Pd, and Mn.

Experimental Section

Catalyst preparation

Ag/SiO_2 was prepared by standard IWI. To dried silica gel (Aldrich 60752; 950 mg), an aqueous solution of $AgNO_3$ (78 mg $AgNO_3$ in 750 µL distilled water) was added under vigorous stirring. After equilibration at RT (0.5 h), the Ag-impregnated silica was dried in static air at 100 °C (16 h) and calcined in static air (1–5 °C min^{-1} 500 °C, 2 h).

Modifications to the preparation procedure: (1) NaOH pretreatment: 0.1 M NaOH aqueous solution (5 mL g_{silica}^{-1}) was stirred with silica for 2 h. The supernatant was removed by centrifugation (1000 rpm), and the solid was washed with distilled H_2O (7×, 1000 rpm), dried (80 °C), and calcined; (2) wet impregnation: distilled H_2O (1.5 mL) was added to silica gel before impregnation, and the material was equilibrated for 1 h at RT; (3) vacuum drying: The silica gel was treated at RT for 16 h at 10 mbar; (4) freeze-drying: the silica gel was frozen at −20 °C for 4 h and cooled in liquid N_2 for 1 h, followed by freeze-drying for 4 h at 0.3 mbar; (5) fluidized-bed drying: the impregnated powder (200 mg) was transferred to a tubular quartz reactor (∅ = 1 cm), and two quartz-wool plugs were used to create a homogeneous flow through the bed and to prevent the powder from blowing out. A controlled flow of 30 mL min^{-1} 80% N_2 20% O_2 was used, and the oven was heated to 100 °C (10 °C min^{-1}) for 8 h; (6) fluidized-bed calcination: the dry powder (200 mg) was heated in a tubular quartz reactor under 30 mL min^{-1} of 80% N_2 and 20% O_2 at a rate of 1 °C min^{-1} to 500 °C for 2 h.

Characterization

Optical microscopy images were obtained from the eyepieces by using an adapter from Micro-Tech-Lab (Austria) to connect a Canon EOS5D color camera to an Olympus BX51 Upright microscope with a standard mercury lamp equipped with infinity corrected air objectives 4× (0.16 N.A.) and 20× (0.40 N.A.). Overview images of the powder bed were obtained by using a Leica (M165FC) stereomicroscope. Color indexing is described in detail in Ref. [2]. Briefly, images were adjusted to obtain optimal contrast and brightness. The mean 8-bit value in the red channel was used to increase the sensitivity towards transparent, light yellow, and yellow granules. N_2 adsorption and desorption isotherms were measured by using a Micromeritics 3Flex 3500 physisorption instrument at 77 K. The sample was degassed before measurement at 423 K for 6 h under vacuum (10–2 mbar). The pore size distribution

was calculated using the Barrett–Joyner–Halenda (BJH; Harkins and Jura thickness curve and Faas correction, 3Flex 3.00 software).

Catalysis

Bulk hydrogenation reactions were performed by using high-pressure 15 mL TOP reactors (30 min, 100 °C, 20 bar of H_2, 2 mol% of Ag, 0,13 M 4-nitrostyrene in EtOH, 500 rpm). The reaction products were analyzed by using GC (Shimadzu, CP-Sil 5, FID detector), and tetradecane was added as internal standard for quantitative GC analysis. The compounds were identified by using GC–MS (Agilent, HP-1, MS).

Acknowledgements

The authors thank the Research Foundation—Flanders (FWO) (PhD scholarship to E.P.) and Belspo (IAP-VII/05). P.E.d.J. and J.E.v.d.R. acknowledge funding from the Netherlands Organization for Scientific Research (NOW-Vici 16.130.344) and K.P.d.J. from the European Research Council (EU FP7 ERC Advanced Grant no. 338846).

Conflict of interest

The authors declare no conflict of interest.

Keywords: heterogeneous catalysis · nanoparticles · silver · supported catalysts · synthesis design

[1] J. Zečević, A. M. J. van der Eerden, H. Friedrich, P. E. de Jongh, K. P. de Jong, *ACS Nano* **2013**, *7*, 3698–3705.
[2] E. Plessers, I. Stassen, S. P. Sree, K. P. F. Janssen, H. Yuan, J. Martens, J. Hofkens, D. De Vos, M. B. J. Roeffaers, *ACS Catal.* **2015**, *5*, 6690–6695.
[3] P. Munnik, P. E. de Jongh, K. P. de Jong, *Chem. Rev.* **2015**, *115*, 6687–6718.
[4] G. Ertl, H. Knözinger, F. Schüth, J. Weitkamp, *Handbook of Heterogeneous Catalysis*, Wiley-VCH, Weinheim, **2008**.
[5] R. J. White, R. Luque, V. L. Budarin, J. H. Clark, D. J. Macquarrie, *Chem. Soc. Rev.* **2009**, *38*, 481–494.
[6] K. P. de Jong, *Synthesis of Solid Catalysts*, Wiley-VCH, Weinheim, Germany, **2009**.
[7] R. Dinnebier, S. Billinge, *Powder Diffraction: Theory and Practice*, The Royal Society Of Chemistry, Cambridge, **2008**.
[8] M. Quinten, *Appl. Phys. B* **2001**, *73*, 317–326.
[9] J. Lyu, J. Wang, C. Lu, Q. Zhang, X. He, X. Li, *J. Phys. Chem. C* **2014**, *118*, 2594–2601.
[10] K. Arve, H. Kannisto, H. H. Ingelsten, K. Eränen, M. Skoglundh, D. Y. Murzin, *Catal. Lett.* **2011**, *141*, 665–669.
[11] G. Corro, U. Pal, E. Ayala, E. Vidal, *Catal. Today* **2013**, *212*, 63–69.
[12] H. Wei, C. Gomez, J. Liu, N. Guo, T. Wu, R. Lobo, L. Christopher, R. Lobo-Lapidus, C. L. Marshall, J. T. Miller, R. J. Meyer, *J. Catal.* **2013**, *298*, 18–26.
[13] K. Shimizu, Y. Miyamoto, A. Satsuma, *J. Catal.* **2010**, *270*, 86–94.
[14] G. Prieto, J. Zečević, H. Friedrich, K. P. de Jong, P. E. de Jongh, *Nat. Mater.* **2013**, *12*, 34–39.
[15] J. Zecevic, G. Vanbutsele, K. P. de Jong, J. A. Martens, *Nature* **2015**, *528*, 245–248.
[16] B. M. Weckhuysen, *Angew. Chem. Int. Ed.* **2009**, *48*, 4910–4943; *Angew. Chem.* **2009**, *121*, 5008–5043.
[17] S. Kalirai, U. Boesenberg, G. Falkenberg, F. Meirer, B. M. Weckhuysen, *ChemCatChem* **2015**, *7*, 3674–3682.
[18] H. Matsui, N. Ishiguro, K. Enomoto, O. Sekizawa, T. Uruga, M. Tada, *Angew. Chem. Int. Ed.* **2016**, *55*, 12022–12025; *Angew. Chem.* **2016**, *128*, 12201–12204.
[19] N. Ishiguro, T. Uruga, O. Sekizawa, T. Tsuji, M. Suzuki, N. Kawamura, M. Mizumaki, K. Nitta, T. Yokoyama, M. Tada, *ChemPhysChem* **2014**, *15*, 1563–1568.
[20] W. Cha, Y. Liu, H. You, G. B. Stephenson, A. Ulvestad, *Adv. Funct. Mater.* **2017**, *27*, 1700331.
[21] Morbidelli, A. Gavriilidis, A. Varma, *Catalyst Design: Optimal Distribution of Catalyst in Pellets, Reactors, and Membranes*, Cambridge University Press, Cambridge, **2001**.
[22] T. Vergunst, F. Kapteijn, J. A. Moulijn, *Appl. Catal. A* **2001**, *213*, 179–187.
[23] X. Liu, J. G. Khinast, B. J. Glasser, *Chem. Eng. Sci.* **2012**, *79*, 187–199.
[24] J. R. Sietsma, H. Friedrich, A. Broersma, M. Versluijs-Helder, A. J. van Dillen, P. E. de Jongh, K. P. de Jong, *J. Catal.* **2008**, *260*, 227–235.
[25] T. M. Eggenhuisen, H. Friedrich, F. Nudelman, J. Zecevic, N. A. J. M. Sommerdijk, P. E. de Jongh, K. P. de Jong, *Chem. Mater.* **2013**, *25*, 890–896.
[26] P. Munnik, P. E. de Jongh, K. P. de Jong, *J. Am. Chem. Soc.* **2014**, *136*, 7333–7340.
[27] Y. Sun, Y. Xia, *Analyst* **2003**, *128*, 686.
[28] S.-Y. Lee, R. Aris, *Catal. Rev. Sci. Eng.* **1985**, *27*, 207–340.
[29] J. Park, J. Regalbuto, *J. Colloid Interface Sci.* **1995**, *175*, 239–252.
[30] M. Kosmulski, *Chemical Properties of Material Surfaces*, Marcel Dekker, New York, Basel, **2001**.
[31] S. H. Behrens, D. G. Grier, *J. Chem. Phys.* **2001**, *115*, 6716–6721.
[32] T. M. Eggenhuisen, M. J. Van Steenbergen, H. Talsma, P. E. de Jongh, K. P. de Jong, *J. Phys. Chem. C* **2009**, *113*, 16785–16791.
[33] P. Munnik, N. Krans, P. De Jongh, K. De Jong, *ACS Catal.* **2014**, *4*, 3219–3226.
[34] A. Brumby, P. Braumann, K. Zimmermann, F. Van Den Broeck, T. Vandevelde, D. Goia, H. Renner, G. Schlamp, W. Weise, P. T. Tews, *Ullmann's Encycl. Ind. Chem.* **2012**, *33*, 15–94.
[35] J. Hu, W. Cai, H. Zeng, C. Li, F. Sun, *J. Phys. Condens. Matter* **2006**, *18*, 5415–5423.
[36] A. Lekhal, B. J. Glasser, J. G. Khinast, *Chem. Eng. Sci.* **2001**, *56*, 4473–4487.
[37] N. Liv, C. A. Zonnevylle, A. C. Narvaez, A. P. J. Effting, P. W. Voorneveld, M. S. Lucas, J. C. Hardwick, R. A. Wepf, P. Kruit, J. P. Hoogenboom, *PLoS One* **2013**, *8*, e55707.
[38] E. Debroye, J. Van Loon, X. Gu, T. Franklin, J. Hofkens, K. P. F. Janssen, M. B. J. Roeffaers, *Part. Part. Syst. Charact.* **2016**, *33*, 412–418.

Manuscript received: May 8, 2017
Revised manuscript received: July 31, 2017
Accepted manuscript online: August 8, 2017
Version of record online: November 23, 2017